Macromolecules

ARTICLE

pubs.acs.org/Macromolecules

SCFT Simulations of an Order−Order Transition in Thin Films of Diblock and Triblock Copolymers

Vindhya Mishra,[†] Glenn H. Fredrickson,[†,‡] and Edward J. Kramer*[,†,‡]

[†]Department of Chemical Engineering and [‡]Department of Materials, University of California, Santa Barbara, Santa Barbara, California 93106, United States

Supporting Information

ABSTRACT: We have used self-consistent field theory (SCFT) simulations to investigate the effect of film thickness and chain architecture on the temperature-dependent sphere to cylinder order−order transition in diblock and triblock copolymers. While the order−order transition temperature (OOT) for bulk phases depends only on the volume fraction for a particular block copolymer, for thin films we find a strong dependence on film thickness and the nature of chains forming the surface wetting layer (i.e., ends vs mid-monomers). Our studies show that subtle differences in the packing frustration of the spherical and cylindrical phases as well as the higher configurational entropy of free chain ends at the surface are sufficient to drive the equilibrium configuration in thin films away from the stable bulk structure. These contributions to the free energy that arise in thin films but are absent in bulk cause the thin film OOT to be shifted from the bulk OOT by $\Delta\chi N \sim 5$.

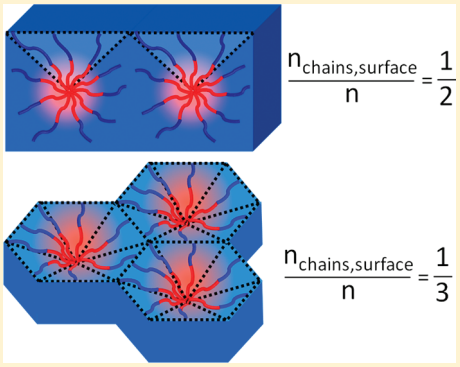

INTRODUCTION

As the equilibrium behavior of block copolymer melts has been well established,[1−5] one can predict the resulting microstructure based on chain architecture, the strength of interaction between the component blocks, and their relative fraction with a reasonably good degree of accuracy. When sufficient mobility is imparted to the block copolymer chains (either by suitable thermal treatment or by exposure to solvent vapor), the chains spontaneously self-assemble into component-rich domains. The shape and arrangement of these microdomains are established by free energy minimization. For block copolymer melts, the two primary contributors to the free energy are the unfavorable contacts between dissimilar chains, which favors domains with uniform interfacial curvature, and redistribution of polymer chains to maintain uniform monomer density, which favors uniform stretching of block copolymer chains. For compositionally asymmetric blocks, these two conditions cannot be simultaneously satisfied, which gives rise to frustration in the resulting lattice arrangement.[6−8] Furthermore, when block copolymers are cast as films, the thickness of the film and the surface energies of the component blocks exert additional influences on the microdomain structure. For example, preferential wetting of one block over the other is typically observed at the top and bottom interfaces of substrate-supported films. This not only induces an ordering of the structure perpendicular to the interfaces[9−11] but also causes a loss of configurational entropy for the chains near the surface.[12] As a result, deviations from bulk equilibrium behavior are expected in thin films.[13−15] There have been several reports of morphological shifts or domain reorientation as a function of film thickness and surface energies.[16,17] There have also been some studies for parallel lamella and cylinder forming systems looking at the effect of film thickness that is incommensurate with the natural periodicity.[18−20]

Compositionally asymmetric block copolymers with microdomains layered parallel to the substrate show remarkable sensitivity to changes in film thickness, even when the film thickness is nearly commensurate with the natural periodicity. For example, spherical morphology block copolymer undergoes changes in microdomain symmetry from hexagonal close packed (HCP) to face centered orthorhombic (FCO) to body centered cubic (BCC) depending on film thickness[21] due to competition between packing frustration of the majority block in the HCP lattice and the surface preference for a hexagonal arrangement.[22] Apart from microdomain shape and arrangement, the order−disorder transition temperature is also affected by film thickness. Hammond et al. observed that monolayers of cylindrical morphology block copolymers melt at a lower temperature compared to the bulk state.[23] Anastasiadis and co-workers observed that surface effects can induce ordering even above the order−disorder transition temperature,[24] a finding that had been predicted theoretically.[25] There has been comparatively less theoretical work on the equilibrium behavior of multilayer films of compositionally asymmetric block copolymers, primarily because they are analytically intractable and typically require three-dimensional simulations that can be computationally expensive.

Received: February 10, 2011
Revised: May 19, 2011
Published: June 16, 2011

Another degree of complexity is introduced when the composition lies at or near the phase boundary of two different morphologies. Such block copolymers can exhibit an order−order transition temperature where a change in microdomain shape is induced by changes in temperature; this may occur near or far from the order−disorder transition. Sohn and co-workers recently performed a careful experimental study of the equilibrium morphology in thin films (<5 layers) of one such system of diblock and triblock copolymers that undergo a sphere to cylinder transition upon increasing temperature in the bulk.[26] They characterized the morphology of thin films of poly(styrene-*b*-ethylene-*r*-butylene) (SEB) and poly(styrene-*b*-ethylene-*r*-butylene-*b*-styrene) (SEBS) copolymers (volume fraction of S $\varphi_S = 0.14$) annealed below and above the bulk order order transition (OOT) temperature as a function of film thickness. They found that in case of the SEBS triblock the thin film morphology was always spherical for up to five layers of spheres for the temperature range studied (±25 °C from the bulk OOT temperature). However, the diblock film morphology at all temperatures was found to be cylindrical, except for film thicknesses smaller than a monolayer of cylinders. Thus, in the thin film regime the OOT for SEB diblocks is increased relative to the bulk OOT, while for SEBS triblocks it is depressed by at least 10 °C relative to the bulk.

In this study we used self-consistent field theory[2,27,28] to predict how film thickness will affect the sphere to cylinder order−order transition temperature for diblock and triblock copolymers. SCFT has been extensively used to predict the equilibrium behavior of copolymer melts in the past[29−31] and has also been successfully adopted for thin films.[19,32−34] Building on the experimental work by Sohn and co-workers, our aim was not only to get a theoretical confirmation of the experimental results but also to identify the driving force for the transition. Note that since we are interested in differences in equilibrium behavior of thermally annealed films, we will not be considering transitions occurring in kinetically trapped systems, that are not captured by SCFT.

SELF-CONSISTENT FIELD THEORY SIMULATIONS

SCFT simulations were carried out for a linear AB copolymer and two triblock copolymers with architectures ABA and BAB, where "B" is the majority component. The approach followed here is similar to the formalism by Bosse et al.[35] and Cochran et al.[36] The salient features are outlined here for completeness. Self-consistent field theory calculates the constrained partition function $q(\mathbf{r},s)$ for a single polymer molecule modeled as a continuous Gaussian chain of contour length N, where $0 \leq s \leq N$, in an inhomogeneous potential field w. This chain propagator obeys the modified diffusion equation

$$\frac{\partial q(\mathbf{r},s)}{\partial s} = \nabla^2 q(\mathbf{r},s) - w_i(\mathbf{r}) q(\mathbf{r},s) \tag{1}$$

where i = A for $s < \varphi_A$ and i = B for $s > \varphi_A$ for the diblock case, with a similar extension to the triblock case, where φ_A is the A block volume fraction. The solution of eq 1 with the initial condition $q(\mathbf{r},0) = 1$ gives $q(\mathbf{r},s)$.

To mimic thin film conditions, we utilized a "masking" technique detailed in an earlier paper[33] to confine the polymer to a thin film bound by planar interfaces by imposing a "wall" density field that expels the polymer from the interface. The wall is denoted by the subscript "W". The standard field theoretic form of the Hamiltonian in the canonical ensemble

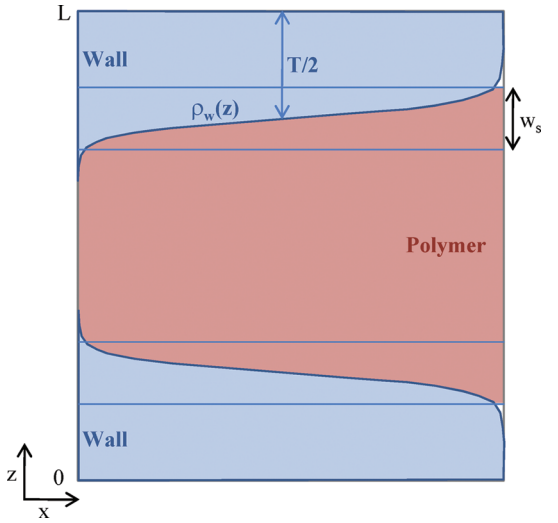

Figure 1. Schematic of the simulation volume showing the shape of the wall profile.

was employed

$$\frac{H}{nk_BT} = \frac{1}{V}\int d^3\mathbf{r}\,[\chi_{AB}\rho_A\rho_B N + \chi_{AW}\rho_W\rho_A N + \chi_{BW}\rho_W\rho_B N - \rho_A w_A - \rho_B w_B - p(1-\rho_A-\rho_B-\rho_W) - \ln Q] \tag{2}$$

where n is the number of chains, V is the volume accessible to the polymers, χ_{XY} is the interaction parameter between species X and Y, ρ_X is a normalized density or an equivalent volume fraction of component X, w_X is the potential field conjugate to species X, p is the pressure, and Q is the partition function of a single chain which is related to the propagator $q(\mathbf{r},s)$ by the expression

$$Q = \frac{1}{V}\int d\mathbf{r}\, q(\mathbf{r},1) \tag{3}$$

The species chemical potential fields can be reformulated in the form of a pressure field $w_+ = (w_A + w_B)/2i$ and an exchange potential field $w_- = (w_B - w_A)/2$. The term $p(1-\rho_A-\rho_B-\rho_W)$ enforces melt incompressibility by appropriate choice of the pressure field p.

$$\rho_A + \rho_B + \rho_W = 1 \tag{4}$$

This constraint, coupled with an appropriate wall density profile, limits the polymer to be confined as a thin film in the normal direction z.[19,22,33] The shape of the wall density profile was chosen to be a smooth tanh function

$$\rho_W(\mathbf{r}) = \frac{1}{2}\left(1 + \tanh\left(2\frac{\left((T+L) - \left|z - \frac{1}{2}L\right|\right)}{w_s}\right)\right) \times \tanh\left(2\frac{\left((T+L) + \left|z - \frac{1}{2}L\right|\right)}{w_s}\right) \tag{5}$$

where w_s, which we will refer to as the wall thickness, is the width of the interfacial region between the wall and polymers.

dx.doi.org/10.1021/ma200297f |*Macromolecules* 2011, 44, 5473–5480

A schematic of the simulation volume is shown in Figure 1, where T is the wall width and L is the distance between the two confining walls. For our simulations we fixed w_s to be $0.5R_g$ and T to be $0.75R_g$, where R_g is the radius of gyration of the polymer, while L was varied in steps of about $0.2R_g$.

The Hamiltonian of eq 2 was analyzed for saddle points in the mean-field limit of the above field theory. We searched for potential fields that gave the spatial distribution of segments of type A and B with the lowest free energy per chain, subject to the local incompressibility condition (eq 4). For sphere-forming systems, simulations were carried out in three dimensions, whereas for the parallel cylinder forming system, a 2D simulation was deemed sufficient. All the fields were represented using a plane wave basis and sampled on a uniform grid with a spatial resolution of least $0.125R_g$ in the lateral x and y and normal z direction. Periodic boundary conditions were imposed in the lateral directions. For the normal direction, periodic boundary conditions with period L were imposed on the mask. The wetting conditions on the two film surfaces defined by the mask were controlled by the choice of χ_w parameters. We examined both symmetric boundary conditions where the majority block B was assumed to have a preferential affinity for the wall, as well as asymmetric boundary conditions where the A and B blocks segregate to opposing walls. The pseudospectral operator splitting algorithm,[37,38] known to have second-order accuracy in the chain contour step size Δs, was used with a step size of 0.005 and fast Fourier transforms to solve the modified diffusion equation (eq 1). A semi-implicit Seidel (SIS) field relaxation scheme[39] was used to update the field configurations. The unit cell parameters in the plane of the film were simultaneously relaxed using an explicit scheme to minimize the local microscopic stress, while the film thickness was specified in the normal direction through the mask function.

The volume fraction φ_A of the minority A block was fixed in our studies to 0.14. The OOT temperatures (χN values) in bulk for diblock and triblock architectures were determined by carrying out the corresponding unit cell calculations in absence of any confining walls. The free energies per chain for film thickness up to $8R_g$ or three layers of microdomains were calculated for spherical and cylindrical morphologies. In practice, the film can relax to a thickness that minimizes its free energy by forming island and hole structures, while conserving the total polymer volume. The "equilibrium" thickness that satisfied this requirement was extracted using a double tangent construction on the effective film surface tension σ which is proportional to $d(f_{film} - f_{bulk})$, where d is the polymer film thickness L-T;[19] the details of this method are given in the Supporting Information. The film thickness was varied in steps of at least $0.2R_g$ (with finer steps near the minima) in order to find the surface tension minima corresponding to different number of layers, as $d_{eq,monolayer} \neq d_{eq,bilayer} \neq d_{eq,bulk}$. The free energy per chain at these equilibrium thicknesses for spherical and cylindrical morphology were then compared to determine the preferred morphology. Field iterations were carried out until the magnitude of the force arising from the pressure field was below $10^{-4.5}k_BT$ per chain, and the force from the exchange potential field was below $10^{-6}k_BT$ for thin film 3D simulations and below $10^{-10}k_BT$ for bulk and 2D simulations. The higher degree of error in the pressure field in the thin film case arises due to the "wall" confinement, which causes the pressure field to peak sharply at the film surfaces, leading to slow convergence of the l_1 norm of the saddle point equations. For bulk state simulations (denoted with a subscript b), the corresponding unit cell calculations were carried out in the absence of any confining walls, which allowed for better convergence and highly accurate free energy values.

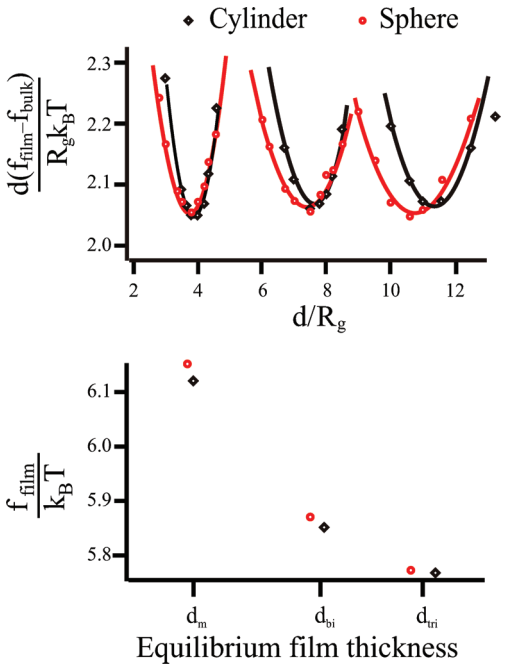

Figure 2. Top: Surface excess free energy per chain for cylindrical and spherical morphologies for the AB diblock architecture as a function of film thickness at the bulk order-order transition temperature. The solid lines are polynomial fits to the data points. Bottom: Comparison between the free energy for spherical and cylindrical morphologies at the respective equilibrium film thickness shows that the cylindrical morphology has lower free energy.

Connections with Experimental Work. The copolymer used by Sohn and co-workers was a styrene-ethylene-*r*-butylene system (SEB), the Flory−Huggins interaction parameter for which is $\chi = 0.02 + 24/T$ for a mer volume $v = 10^{-22}$ cm^3 and the bulk OOT was reported to be 143 °C.[40] They experimentally examined thickness dependent equilibrium morphologies at 125 and 165 °C. The effective N that we employed for the simulations was determined by dividing the theoretically determined χN_{OOT} by the value of χ at 143 °C. Simulations then spanned $\Delta\chi N$ of at least $0.007N$ in order to mimic the experimental conditions. The experiments report that for both the diblock and triblock architectures, the lower surface energy majority EB block preferentially wets the polymer−air interface, while a styrene wetting layer is formed next to the substrate. For a majority of the simulations, we employed the computationally less expensive geometry of symmetric wetting conditions as we expected that the effect of asymmetric walls would be to simply produce a shift in the free energy due to the additional enthalpic contributions. The symmetric wetting condition was implemented by setting $\chi_{WA} = \chi_{AB}$ and $\chi_{WB} = 0$, which resulted in the majority B block migrating to the walls. In addition, we also implemented asymmetric boundary conditions for monolayer systems (with the A block wetting the substrate and the B block wetting the film−air interface) to investigate if the boundary conditions affected the equilibrium behavior.

RESULTS AND DISCUSSION

We first present results for an AB diblock with $\varphi_A = 0.14$. The bulk OOT was determined by searching for the value of χN at

dx.doi.org/10.1021/ma200297f |*Macromolecules* 2011, 44, 5473–5480

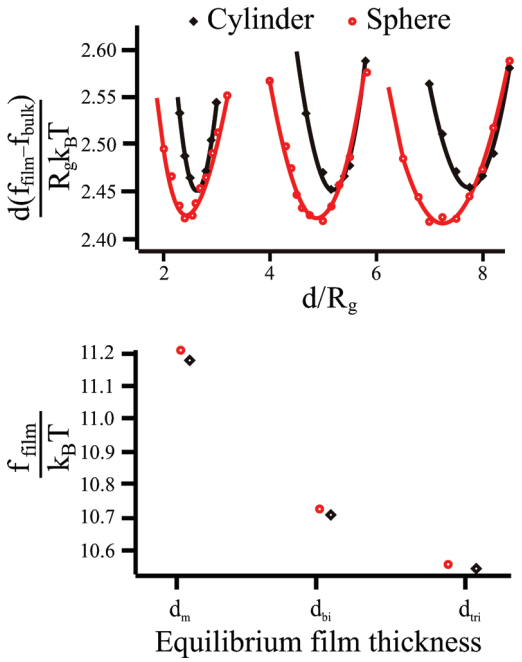

Figure 3. Top: Surface excess free energy per chain for cylindrical and spherical morphologies for an ABA triblock as a function of film thickness at the bulk order-order transition temperature. The solid lines are polynomial fits to data points. Bottom: Comparison between the free energy for spherical and cylindrical morphologies at the respective equilibrium film thickness shows that the cylindrical morphology has lower free energy.

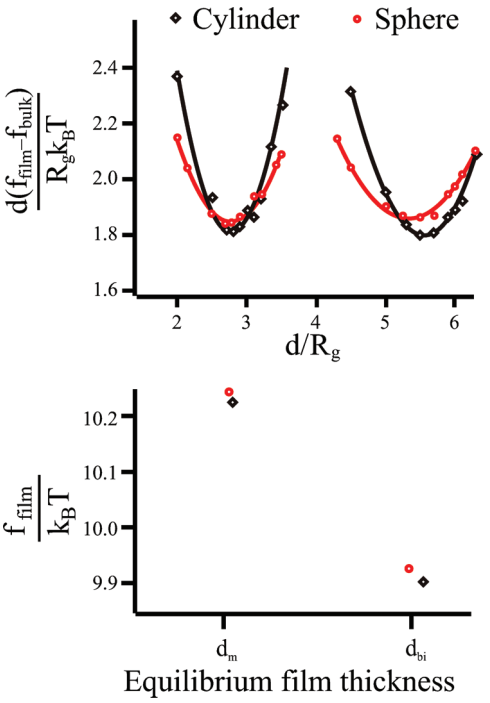

Figure 4. Top: Surface excess free energy per chain for cylindrical and spherical morphologies for a BAB triblock as a function of film thickness at the bulk order-order transition temperature. Bottom: Comparison between the free energy for spherical and cylindrical morphologies at the respective equilibrium film thickness shows that the cylindrical morphology has lower free energy.

which the difference in free energy per chain "f" between bulk phase spherical and cylindrical morphologies $\Delta f_b = f_{b,c} - f_{b,s}$ was zero and was found to be 62.5 for the AB diblock. However, thin film simulations carried out at this χN did not show this degeneracy between the cylindrical and spherical phases. The equilibrium film thickness for monolayer, bilayer, and trilayer films was found by the double-tangent construction methodology as detailed in the Supporting Information. Figure 2 shows plots of the surface excess free energy per chain $\sigma = d(f_{film} - f_{bulk})/(R_g k_B T)$ at the bulk OOT for spherical and cylindrical morphology films. Symmetric boundary conditions were used for this calculation. Comparing the free energy per chain of the two morphologies at their respective equilibrium thickness, we find that at the bulk OOT temperature ($\chi N \sim 62.5$) where $\Delta f_b = 0$, $\Delta f_{monolayer} = f_{monolayer,s} - f_{monolayer,c} = 0.029 \pm 0.001\ k_B T$, $\Delta f_{bilayer} = 0.007 \pm 0.001\ k_B T$, and $\Delta f_{trilayer} = 0.001 \pm 0.001\ k_B T$ on a per chain basis. This implies that the OOT shifts to higher temperatures as the film thickness is decreased. The cylindrical phase in the AB diblock is preferentially stabilized for monolayer, bilayer, and trilayer films up to higher temperatures compared to the bulk. Simulations carried out at temperatures above and below the OOT show that as the film thickness is increased, the OOT temperature approaches that of the bulk. Compared to $\chi N = 62.5$ for bulk, for a monolayer of microdomains the OOT occurred at $\chi N = 57$. For the SEB system this $\Delta\chi N$ corresponds to a difference of about 20 °C between the OOT temperatures of bulk and a monolayer; however, for systems with a weaker temperature dependence of the χ parameter, this change will be even larger.

In order to determine if these free energy differences are sufficient to drive a morphological change experimentally, we examined the experimental system SEB studied by Sohn and co-workers where they report bulk OOT for SEB diblock to be 143 °C and the bulk equilibrium morphologies at 125 and 165 °C to be cylindrical and spherical, respectively. According to our bulk state simulations the free energy differences per chain $f_{b,c} - f_{b,s}$ at these temperatures are $-0.001 k_B T$ and $0.0022 k_B T$, respectively. This implies that free energy differences of the order of $10^{-3} k_B T$ per chain are sufficient to drive morphological transitions. Hence, at the bulk OOT temperature for the AB diblock, we should expect that cylindrical morphology will be observed in thin films.

The second architecture we investigated was a symmetric ABA triblock copolymer with equal length A blocks and of the same overall A composition as the diblock, i.e., $\varphi_A = 0.14$. Such a polymer could be prepared by coupling the corresponding AB diblocks. The value of χN at which the spherical and cylindrical morphologies of the bulk ABA triblock have the same free energy per chain was determined to be 103.5. For the thin film case, the free energy landscape is again different from that of the bulk with the OOT being shifted to higher temperatures. Figure 3 shows the surface excess free energy per chain at the bulk order−order transition temperature plotted as a function of film thickness. We find that at the bulk OOT $\Delta f_{monolayer} = 0.032 \pm 0.001 k_B T$, $\Delta f_{bilayer} = 0.017 \pm 0.001 k_B T$, and $\Delta f_{trilayer} = 0.014 \pm 0.001 k_B T$ on a per chain basis. Interestingly, the surface excess free energy or "surface tension" for the cylindrical morphology is higher than the spherical morphology, but at the equilibrium film thickness the free energy per chain is lower for the cylindrical morphology, as the equilibrium film thickness for the cylindrical morphology is larger than the spherical morphology.

The third copolymer system we investigated was a triblock with reversed architecture, i.e., the BAB form with φ_A again fixed

Table 1. Equilibrium Film Thickness and Free Energy Differences between Monolayers of Spherical and Cylindrical Morphologies for Different Chain Architectures and Wetting Conditions

	d_{sphere} (R_g)	d_{cyl} (R_g)	$f_{sph} - f_{cyl}$ (k_BT)
symmetric boundary conditions			
AB diblock	3.65	3.84	0.029
ABA triblock	2.5	2.65	0.032
BAB triblock	2.67	2.86	0.037
asymmetric boundary conditions			
AB diblock	5.83	5.97	0.010
ABA triblock	4.27	4.29	−0.008

at 0.14. At the bulk OOT (which was determined to be $\chi N = 127$), the difference in free energy between the spherical and cylindrical morphologies in thin films was nonzero and was found to be $\Delta f_{monolayer} = 0.037 \pm 0.001 k_BT$ and $\Delta f_{bilayer} = 0.025 \pm 0.002 k_BT$ on a per chain basis. The surface excess free energy curves used to determine the equilibrium film thickness are shown in Figure 4. Again, the transition temperature shifts toward the bulk OOT upon increasing thickness.

Asymmetric Wetting Conditions. The above results were for a system that exhibits symmetric wetting conditions with the majority block showing preferential attraction to the polymer−air and polymer−substrate interfaces. Since the experimental system of Sohn et al. exhibits asymmetric wetting behavior, we implemented the same in our calculations for monolayers of the diblock and ABA triblock. The interaction parameter between a wall and its corresponding wetting block was set equal to zero, and that between the wall and the nonwetting block was set equal to χ_{AB}. We find that for the diblock architecture the equilibrium morphology was the same irrespective of the nature of the boundary conditions; however, the free energy difference between the two morphologies was reduced, which implies that the shift in OOT temperature compared to the bulk is also reduced. With symmetric boundary conditions as shown earlier, the diblock cylindrical morphology free energy at its equilibrium film thickness is lower than that for spheres at its equilibrium film thickness by $0.029 k_BT$ per chain. With asymmetric boundary conditions, the difference in the free energy between spheres and cylinders at their respective equilibrium thickness is reduced to $0.01 k_BT$ per chain, with the cylindrical morphology still being the preferred morphology (the relevant surface energy graphs are shown in the Supporting Information). However, for the ABA triblock architecture, the relative stability of the two morphologies was reversed when the nature of the boundary conditions were changed. The equilibrium morphology of an ABA triblock monolayer with symmetric boundary conditions at the bulk OOT temperature is cylindrical, with the free energy of the cylindrical morphology being lower than that of the spherical morphology by $0.079 k_BT$ per chain. However, with asymmetric wetting conditions the equilibrium free energy in the spherical morphology becomes slightly lower than that of cylindrical morphology by $0.008 k_BT$ per chain. Hence, the relative free energies of the spherical and cylindrical morphologies depend on the nature of the boundary conditions. From our calculations, one can infer that while the effect of asymmetric boundary conditions is to reduce the free energy per chain for both the spherical and cylindrical morphologies, the energetic relief is higher for the spherical morphology. In case of the AB diblock, the difference in free energies per chain $f_{sph,symm} - f_{sph,asymm} = 0.13 k_BT$ while $f_{cyl,symm} - f_{cyl,asymm} = 0.11 k_BT$ and for the ABA triblock $f_{sph,symm} - f_{sph,asymm} = 0.27 k_BT$, whereas $f_{cyl,symm} - f_{cyl,asymm}$ is $0.18 k_BT$. Note that the SEB/SEBS experimental system studied by Sohn et al. exhibited asymmetric wetting behavior, and our results with the asymmetric boundary conditions are in good agreement with experimental reports. A summary of the free energy differences for different chain architectures under the two film boundary conditions is tabulated in Table 1.

Table 2. Free Energy Changes Arising from Unit Cell Distortion at the Order−Order Transition Temperature for the AB Diblock and ABA Triblock

	AB diblock			ABA triblock		
$f(k_BT)$	distorted	equilibrium	difference	distorted	equilibrium	difference
$f_{cylinder}$	5.613	5.585	0.028	10.253	10.214	0.039
f_{sphere}	5.612	5.585	0.027	10.251	10.214	0.037
difference	0.001	0	0.001	0.002	0	0.002

Discussion. In order to understand these dramatic changes in thin film behavior compared to the bulk, we considered a number of possible factors that are expected to alter the free energy of the films. First, the shape of the Wigner−Seitz cell of the microdomains in a monolayer is different from that in the bulk. For a monolayer of cylinders, the unit cell shape is square instead of hexagonal in the bulk, whereas a monolayer of spheres are arranged in a hexagonal unit cell in-plane compared to the dodecahedral unit cell of a body centered cubic lattice, which is the preferred symmetry in bulk. A circular unit cell for cylindrical and spherical morphology would be the lowest energy configuration since it eliminates any unfavorable stretching of the corona chains. However, distortion of the unit cell away from this ideal configuration is required in order to form a space-filling structure. One might imagine that a "rounder" unit cell such as the hexagonal unit cell for sphere monolayers would have less frustration than the square unit cell for cylinder monolayers. Strong segregation theory (SST) calculations by Olmsted and Milner[41] have shown that the ratio of free energy per chain for a cylinder with a square Wigner−Seitz cell is 1.063 times that for a cylinder with a hexagonal unit cell, while a sphere in a FCC lattice had free energy 1.005 times that in a BCC lattice. This suggests that the increase in free energy going from the bulk state to a monolayer in the spherical morphology will be less than that of the cylindrical. However, the monolayer unit cell for spherical microdomains is a simple hexagonal lattice (not close packed), and near the OOT the polymer chains are in the weak or intermediate segregation regime. To obtain a better estimate for the free energy increase due to unit cell distortion, we calculated the difference in free energy of bulk simulations of diblock cylinders in square vs hexagonal unit cells and spheres in simple hexagonal vs BCC lattices at the bulk OOT. The results are tabulated in Table 2. Note that this only shows the difference in free energy that arises from a change in the unit cell, it does not take into account surface effects or the truncation of the unit cell at the interfaces, which again would contribute significantly to the packing frustration. We find that the difference $f_{b,c,square} - f_{b,c,hex}$ and $f_{b,s,hcp} - f_{b,s,bcc}$ is nearly identical at the bulk OOT and about $0.027 k_BT$ at the same temperature. Our SCFT calculation deviates from the SST result in estimating the increase in free

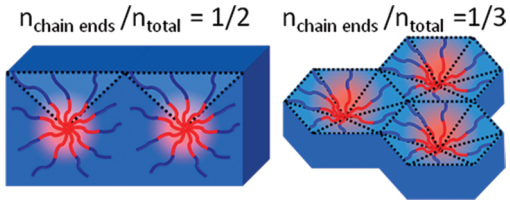

Figure 5. Fraction of polymer chains per unit cell at the top and bottom film surfaces.

energy for the cylindrical morphology—our results predict an increase of 0.5% while the SST states that the increase should be 6%. This discrepancy can be justified as apart from the approximations in the Olmsted and Milner calculation, near the order—order transition temperature ($\chi N = 62.5$), the strong segregation approximation is not likely to be valid. The packing frustration in the spherical morphology HEX unit cell is thus slightly less than the cylindrical morphology square unit cell by $\sim 0.002 k_B T$. Similar results were obtained for the ABA triblock at the corresponding bulk OOT temperature. Hence, according to the SCFT calculations, the increase in free energy for cylinders due to distortion of the unit cell is only slightly higher than that for spheres, although intuitively we expect the difference to be much larger.

Apart from changes in the unit cell, the presence of the surface is also expected to have a significant effect on the free energy. It had been suggested that for triblocks with lower surface energy midblock segments suffer a loss in conformational entropy compared to diblocks as the mid blocks are forced to loop at the surface.[33] However, later works have shown that this 'looping penalty' is not significant,[42] hence that effect is not considered further in our discussion. A recent study shows that a significant surface induced effect is the loss in configurational entropy of polymer segments at the surface, resulting in increased free energy.[42] The contribution of this effect to the free energy per polymer chain can be estimated by

$$(f_{\text{film, surface chains}} - f_{\text{bulk}}) = \frac{a^2 k_B T}{24 d} \int \frac{[\varphi_0'(z)]^2}{\varphi_0(z)} \, dz \qquad (6)$$

where a is the statistical segment length, d is the film thickness, and φ_0 is the polymer volume fraction, which is $1 - \varphi_w$. For the tanh wall profile used in the simulations, this simplifies to

$$(f_{\text{film, surface chains}} - f_{\text{bulk}}) = \frac{a^2 k_B T}{12 w_s d} \qquad (7)$$

Hence, chains in the presence of a surface are expected to lose configurational entropy. However, Wu and co-workers[43] have shown that end monomers of homopolymers placed near a surface incurred a smaller entropic penalty than middle monomers. Furthermore, a recent study[42] has shown that for lamella forming triblock copolymers the distribution of end blocks at a surface is broader compared to the distribution of the midblocks in their respective surface wetting layers. This implies that the end-blocks will have greater configurational entropy than the mid-blocks in their corresponding wetting layer. This entropic gain favoring chain ends over chain middles has been calculated for lamella forming block copolymers with neutral surfaces to be[12,26]

$$f_{\text{ends}} - f_{\text{mid}} = -1.52 \frac{w_s k_B T}{d} \qquad (8)$$

Hence, a larger population of chain ends at the surface will result in lowering the free energy compared to mid-blocks at the

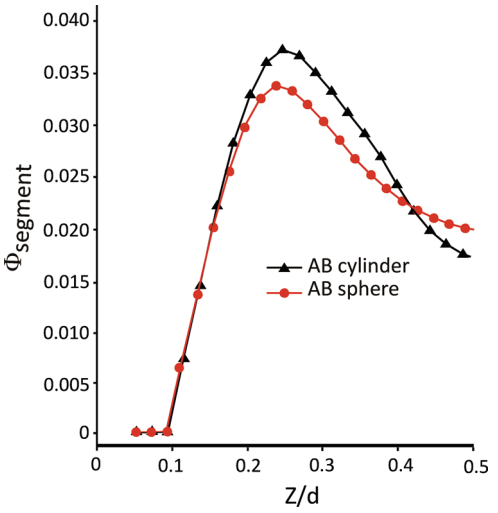

Figure 6. Distribution of chain ends as a function of distance from polymer—wall interface for AB diblock architecture.

surface. While the above expression was obtained for lamella forming systems, the same effect will arise in cylinder and sphere forming block copolymers as well. As pointed out by Sohn et al., while all the chains arising from a microdomain in lamella forming systems are present at the surface, for cylindrical and spherical morphologies the fraction of majority block ends per microdomain that are present at the surface will be at the most 1/2 and 1/3, respectively, shown schematically in Figure 5. This argument relies on the assumption that the area per chain is uniform on the surfaces of the cylindrical and spherical micelles. Accounting for this difference in chain-end population, eq 8 for cylinders is modified to $-0.76 w_s k_B T/d$, while for spheres it becomes $-0.51 w_s k_B T/d$. So, unlike the effect of unit cell distortion, the entropic contribution of chain ends favors cylinders over spheres with an entropic gain which can have a maximum value of $\sim -0.25 w_s k_B T/d$. Note that as this gain is inversely proportional to the film thickness, the relative contribution of the effect will decrease as film thickness increases. It should also be pointed out that this calculation assumes that all the chain ends arising from each microdomain are stretched to occupy the surface, which in practice would be unfavorable. The probability density of finding a polymer chain whose free end is at position $\mathbf{r}$ is given by the chain propagator $q(\mathbf{r},1)$. Hence, the fraction of end segments at a distance z from the wall can be estimated as $\varphi_{\text{segment}}(z) = \int\int dx\, dy\, (q((x,y),0) q_c((x,y),1) + q((x,y),1) q_c((x,y),0))/\int\int\int dx\, dy\, dz (q((x,y,z),0) q_c((x,y,z),1) + q((x,y,z),1) q_c((x,y,z),0))$. Here q_c refers to the reverse propagator which is the solution to the modified diffusion equation (eq 1) with the initial condition $q_c(\mathbf{r},1) = 1$. A plot showing the estimated distribution of the majority B block chain ends near the surface for the spherical and cylindrical morphologies for the AB diblock is shown in Figure 6. One can see that the cylindrical morphology has a greater density of B block chain ends at the surface. Note that the plot shows the fraction of chain ends as a function of distance from the wall normalized by the film thickness which is larger for cylindrical morphology monolayer than for the spheres.

We now examine the combined role of unit cell distortions and surface entropic effects in the context of the systems examined in our simulations. We will first discuss the case of symmetric boundary conditions with the majority block being attracted to

the walls. In case of the diblock, the equilibrium film thickness for a spherical morphology monolayer is found to be $\sim 3.65R_g$ and that for the cylindrical morphology monolayer is $3.84R_g$ (from Table 1). This would result in an entropic gain due to chain ends of $0.0291k_BT$ per chain favoring cylinders. The lower packing frustration of spheres stabilizes the sphere monolayer phase by $0.001k_BT$ per chain over cylinders. Hence, the overall free energy of cylinders will be lower by about $0.029k_BT$ per chain at each interface, so the cylindrical morphology will be favored in thin films. Our simulations, as well as the experimental results of Sohn and co-workers show that cylinders are favored for diblocks within monolayer films, and the free energy difference between cylinders and spheres that we obtain is $0.029 \pm 0.0001k_BT$ per chain, which is close to our estimate based on the packing frustration and surface effects argument. The numbers might be subject to some degree of inaccuracy arising from numerical errors in the thin film simulation and approximations inherent in the application of eq 8 to spherical and cylindrical monolayers. In case of BAB triblock copolymers, the end segments populate the surface, which would favor the cylindrical morphology. Evaluating eq 8 for $w_s = 0.5R_g$ and $d = 2.67R_g$ and $2.8R_g$ for spherical and cylindrical morphologies, respectively, we obtain that the entropic gain is $0.040k_BT$ higher for the cylindrical morphology. Accounting for the lower packing frustration of the spheres and that the two chain ends per mid-block for the BAB architecture, this would imply cylinders being favored by $0.054k_BT$ per chain. This again is close to the value obtained from our simulations ($\sim 0.037 \pm 0.0002k_BT$). The BAB architecture was not studied in Sohn's experimental work. Note that the estimate of free energy difference obtained from SFCT simulations for the BAB triblock is about twice that of the AB triblock, which is consistent since the number of chain ends per chain mids for the BAB triblock is twice that of the AB diblock.

Next, we examine the case of the ABA triblock, the behavior of which we cannot completely explain. As the lower surface energy mid-block B is at the surface, the entropic contribution arising from chain ends favoring cylinders should be absent. While spherical morphology has slightly lower packing frustration than cylindrical morphology ($\sim 0.002k_BT$ per chain), this difference is probably not significant. However, the simulations show that the cylindrical morphology has lower free energy than the spherical phase; hence, there must be another contributing factor that favors the cylindrical morphology. As the simulations embody much more complex physics than reflected in our purely geometrical arguments surrounding unit cell changes and entropy of chain ends, it is possible that there exist certain factors that we have not identified. Note that while the excess surface free energy of the cylindrical and spherical morphologies at the bulk OOT temperatures are nearly equal for the AB diblock and BAB triblock as can be seen in Figures 2 and 4, there is a substantial difference in case of the ABA triblock where the mid-segments populate the surface (Figure 3). Despite the cylindrical morphology having higher excess surface energy per unit area (effectively equilibrium "surface tension") than the spherical morphology, the free energy per chain for the cylindrical morphology is lower as it has a higher equilibrium film thickness. However, the physical driving force behind the preference for cylindrical morphology is not completely clear, and further investigation would be required to understand the cause behind this stabilization.

We also varied the wall thickness for the AB diblock, i.e., the parameter w_s, in order to confirm that the free energy difference changes predictably with wall thickness (as would be expected according to eq 8). For the AB diblock architecture reducing the wall thickness to $0.3R_g$ from $0.5R_g$ reduces the free energy difference to 0.64 times the original, while increasing it to $0.6R_g$ increased the difference by a factor of 1.4. This further supports the hypothesis that morphological transformations in the AB diblock were driven by the entropy of chain ends, rather than other factors such as chain looping. However, when similar calculations were carried out for the ABA triblock, we find that the free energy difference increases with reduction in wall thickness. When the wall thickness was reduced from $0.5R_g$ to $0.3R_g$, the free energy difference increased 2.3 times, while increasing it to $0.6R_g$ reduced the free energy to 0.74 times the original difference. This shows that the width of the surface does play a significant role in the ABA triblock morphology where the mid-blocks populate the surface, but the effect of changing the width is opposite to that for the morphologies where the end-segments populate the surface.

Interestingly, we found that changing the nature of the boundary conditions from symmetric to asymmetric shifts the preference toward the spherical morphology phase. If we compare the degree of segregation for the AB diblock copolymer in a monolayer vs in the bulk by looking at the distribution of the B block in a unit cell along the surface parallel and surface perpendicular axis, we find that while the extent of segregation is nearly identical for the thin film and bulk case along the nearest-neighbor (surface parallel) axis, the thin film is more strongly segregated along the axis perpendicular to the substrate. One can speculate that changing the nature of the boundary conditions will change the breadth of the distribution profile near the surface, which will affect the entropy of the chain ends. Note that eq 8 was obtained for neutral boundary conditions and hence does not include any enthalpic effects.

These studies show that the ability to control nanoscale structure in thin films present additional challenges not present in bulk phases due to confinement effects on equilibrium behavior. Packing frustration arising from distortion of the unit cell in thin films compared to the bulk, the entropy of chain ends at the surface as well as the nature of the wetting layers at the polymer—substrate and polymer air interfaces can drive the equilibrium morphology in thin films away from that of the bulk.

■ ASSOCIATED CONTENT

Ⓢ Supporting Information. Detailed determination of equilibrium morphology using double tangent construction, and the effect of boundary conditions on the free energy differences between the two morphologies. This material is available free of charge via the Internet at http://pubs.acs.org.

■ AUTHOR INFORMATION

Corresponding Author
*E-mail: edkramer@mrl.ucsb.edu.

■ ACKNOWLEDGMENT

We gratefully acknowledge funding from the NSF DMR Contracts DMR-07-04539 and DMR-09-04499 as well as the CSP Technologies Fellowship for partial support of V.M. Use of the MRL Facilities was supported by the MRSEC Program of the National Science Foundation under Contract DMR-0520415. V.M. thanks Su-mi Hur for assistance with the simulations as well as Eric Cochran for the code used for the simulations.

REFERENCES

(1) Cochran, E. W.; Garcia-Cervera, C. J.; Fredrickson, G. H. *Macromolecules* **2006**, *39*, 4264.
(2) Helfand, E.; Tagami, Y. *J. Chem. Phys.* **1972**, *56*, 3592–3692.
(3) Bates, F. S.; Fredrickson, G. H. *Annu. Rev. Phys. Chem.* **1990**, *41*, 525–557.
(4) Bates, F. S.; Schulz, M. F.; Khandpur, A. K.; Förster, S.; Rosedale, J. H.; Almdal, K.; Mortensen, K. *Faraday Discuss.* **1994**, *98*, 7–18.
(5) Förster, S.; Khandpur, A. K.; Zhao, J.; Bates, F. S.; Hamley, I. W.; Ryan, A. J.; Bras, W. *Macromolecules* **1994**, *27*, 6922–6935.
(6) Gruner, S. M. *J. Phys. Chem.* **1989**, *93*, 7562–7570.
(7) Matsen, M. W. *Macromolecules* **1995**, *28*, 5765–5773.
(8) Matsen, M. W.; Bates, F. S. *Macromolecules* **1996**, *29*, 1091–1098.
(9) Anastasiadis, S. H.; Russell, T. P.; Satija, S. K.; Majkrzak, C. F. *Phys. Rev. Lett.* **1989**, *62*, 1852–1855.
(10) Kellogg, G. J.; Walton, D. G.; Mayes, A. M.; Lambooy, P.; Russell, T. P.; Gallagher, P. D.; Satija, S. K. *Phys. Rev. Lett.* **1996**, *76*, 2503–2506.
(11) Coulon, G.; Russell, T.; Deline, V.; Green, P. *Macromolecules* **1989**, *22*, 2581–2589.
(12) Matsen, M. W. *Macromolecules* **2010**, *43*, 1671–1674.
(13) Fasolka, M. J.; Mayes, M. A. *Annu. Rev. Mater. Res* **2001**, *31*, 323–355.
(14) Karim, A.; Singh, N.; Sikka, M.; Bates, F. S.; Dozier, W. D.; Felcher, G. P. *J. Chem. Phys.* **1994**, *100*, 1620–1629.
(15) Krausch, G. *Mater. Sci. Eng., R* **1995**, *14*, 1–94.
(16) Zhang, X.; Berry, B. C.; Yager, K. G.; Kim, S.; Jones, R. L.; Satija, S.; Pickel, D. L.; Douglas, J. F.; Karim, A. *ACS Nano* **2008**, *2*, 2331–2341.
(17) Tsarkova, L.; Knoll, A.; Krausch, G.; Magerle, R. *Macromolecules* **2006**, *39*, 3608–3615.
(18) Knoll, A.; Horvat, A.; Lyakhova, K. S.; Krausch, G.; Sevink, G. J. A.; Zvelindovsky, A. V.; Magerle, R. *Phys. Rev. Lett.* **2002**, *89*, 035501.
(19) Matsen, M. W. *J. Chem. Phys.* **1997**, *106*, 7781–7791.
(20) Fasolka, M. J.; Banerjee, P.; Mayes, A. M.; Pickett, G.; Balazs, A. C. *Macromolecules* **2000**, *33*, 5702–5712.
(21) Stein, G. E.; Kramer, E. J.; Li, X. F.; Wang, J. *Macromolecules* **2007**, *40*, 2453–2460.
(22) Mishra, V.; Hur, S. M.; Cochran, E. W.; Stein, G. E.; Fredrickson, G. H.; Kramer, E. J. *Macromolecules* **2010**, *43*, 1942–1949.
(23) Hammond, M. R.; Cochran, E.; Fredrickson, G. H.; Kramer, E. J. *Macromolecules* **2005**, *38*, 6575–6585.
(24) Anastasiadis, S. H.; Russell, T. P.; Satija, S. K.; Majkrzak, C. F. *Phys. Rev. Lett.* **1989**, *62*, 1852–1855.
(25) Fredrickson, G. H. *Macromolecules* **1987**, *20*, 2535–2542.
(26) Sohn, K. E.; Kojio, K.; Berry, B. C.; Karim, A.; Coffin, R. C.; Bazan, G. C.; Kramer, E. J.; Sprung, M.; Wang, J. *Macromolecules* **2010**, *43*, 3406–3414.
(27) Edwards, S. *Proc. Phys. Soc. London* **1965**, *85*, 613.
(28) Helfand, E.; Sapse, A. M. *J. Chem. Phys.* **1975**, *62*, 1327–1331.
(29) Matsen, M. W.; Schick, M. *Phys. Rev. Lett.* **1994**, *72*, 2660–2663.
(30) Fredrickson, G. H. *The Equilibrium Theory of Inhomogenous Polymers*; Oxford University Press: New York, 2006.
(31) Matsen, M. W. *J. Phys.: Condens. Matter* **2002**, *14*, R21–R47.
(32) Stein, G. E.; Cochran, E. W.; Katsov, K.; Fredrickson, G. H.; Kramer, E. J.; Li, X.; Wang, J. *Phys. Rev. Lett.* **2007**, *98*, 158302.
(33) Khanna, V.; Cochran, E. W.; Hexemer, A.; Stein, G. E.; Fredrickson, G. H.; Kramer, E. J.; Li, X.; Wang, J.; Hahn, S. F. *Macromolecules* **2006**, *39*, 9346–9356.
(34) Pickett, G. T.; Balazs, A. C. *Langmuir* **2001**, *17*, 5111–5117.
(35) Bosse, A. W.; Garcia-Cervera, C. J.; Fredrickson, G. H. *Macromolecules* **2007**, *40*, 9570–9581.
(36) Cochran, E. W.; Garcia-Cervera, C. J.; Fredrickson, G. H. *Macromolecules* **2006**, *39*, 2449–2451.
(37) Rasmussen, K. O.; Kalosakas, G. *J. Polym. Sci., Part B: Polym. Phys.* **2002**, *40*, 1777–1783.
(38) Tzeremes, G.; Rasmussen, K. O.; Lookman, T.; Saxena, A. *Phys. Rev. E* **2002**, *65*, 041806.
(39) Ceniceros, H. D.; Fredrickson, G. H. *Multiscale Model. Simul.* **2004**, *2*, 452–474.
(40) Krishnamoorti, R.; Silva, A. S.; Modi, M. A.; Hammouda, B. *Macromolecules* **2000**, *33*, 3803–3809.
(41) Olmsted, P. D.; Milner, S. T. *Macromolecules* **1998**, *31*, 4011–4022.
(42) Matsen, M. W. *Macromolecules* **2010**, *43*, 1671–1674.
(43) Wu, D. T.; Fredrickson, G. H.; Carton, J.-P.; Ajdari, A.; Leibler, L. *J. Polym. Sci., Part B: Polym. Phys.* **1995**, *33*, 2373–2389.